AGU100 ADVANCING EARTH AND SPACE SCIENCE

JGR

Journal of Geophysical Research: Atmospheres

RESEARCH ARTICLE

10.1029/2018JD028549

Key Points:
- Out-of-sample testing when introducing bias correction approaches is critical
- Biases in trends can dominate uncertainty in estimates of anthropogenic effect on extreme weather
- Calibration on distribution shapes does not guarantee improved skill of attribution statements

Supporting Information:
- Supporting Information S1

Correspondence to:
N. Herger,
nadja.herger@student.unsw.edu.au

Citation:
Herger, N., Angélil, O., Abramowitz, G., Donat, M., Stone, D., & Lehmann, K. (2018). Calibrating climate model ensembles for assessing extremes in a changing climate. *Journal of Geophysical Research: Atmospheres*, *123*, 5988–6004. https://doi.org/10.1029/2018JD028549

Received 19 FEB 2018
Accepted 19 MAY 2018
Accepted article online 27 MAY 2018
Published online 12 JUN 2018

Calibrating Climate Model Ensembles for Assessing Extremes in a Changing Climate

Nadja Herger[1,2], Oliver Angélil[1,2], Gab Abramowitz[1,3], Markus Donat[1,2], Dáithí Stone[4,5], and Karsten Lehmann[6]

[1]Climate Change Research Centre, UNSW, Sydney, New South Wales, Australia, [2]ARC Centre of Excellence for Climate System Science, Sydney, New South Wales, Australia, [3]ARC Centre of Excellence for Climate Extremes, Sydney, New South Wales, Australia, [4]Lawrence Berkeley National Laboratory, Berkeley, CA, USA, [5]Global Climate Adaptation Partnership, Oxford, UK, [6]Satalia, Berlin, Germany

Abstract Climate models serve as indispensable tools to investigate the effect of anthropogenic emissions on current and future climate, including extremes. However, as low-dimensional approximations of the climate system, they will always exhibit biases. Several attempts have been made to correct for biases as they affect extremes prediction, predominantly focused on correcting model-simulated distribution shapes. In this study, the effectiveness of a recently published quantile-based bias correction scheme, as well as a new subset selection method introduced here, are tested out-of-sample using model-as-truth experiments. Results show that biases in the shape of distributions tend to persist through time, and therefore, correcting for shape bias is useful for past and future statements characterizing the probability of extremes. However, for statements characterized by a ratio of the probabilities of extremes between two periods, we find that correcting for shape bias often provides no skill improvement due to the dominating effect of bias in the long-term trend. Using a toy model experiment, we examine the relative importance of the shape of the distribution versus its position in response to long-term changes in radiative forcing. It confirms that the relative position of the two distributions, based on the trend, is at least as important as the shape. We encourage the community to consider all model biases relevant to their metric of interest when using a bias correction procedure and to construct out-of-sample tests that mirror the intended application.

1. Introduction

Observations and climate models show an increase in the frequency and intensity of hot and wet extremes and a decrease in the frequency and intensity of cold extremes, as associated regional mean temperatures increase (Alexander et al., 2006; Collins & Knutti, 2013; Hartmann et al., 2013; Lewis & King, 2015; Seneviratne et al., 2012). These changes coincide with a period of rapid increase in atmospheric CO_2 concentrations as a consequence of anthropogenic industrialization. Given the current state of rapid change, the climate science community, governments, the public, and news media have become interested in how human interference with the climate system has affected various characteristics of extreme weather. This includes current changes in occurrence probability (Herring et al., 2014, 2015, 2016; Peterson et al., 2012, 2013)—a field known as *event attribution*—as well as 21st century (and beyond) projections of extremes (Sillmann et al., 2013) and the impacts associated with them (Patz et al., 2005). Since the 2015 Paris Agreement, which aims to pursue efforts to limit warming to 1.5°C above preindustrial levels and hold the increase in the global average temperature to well below 2°C, studies comparing projections of future extremes between 1.5 and 2°C worlds have grown in popularity (King & Karoly, 2017; King et al., 2017; Lewis & King, 2017; Perkins-Kirkpatrick & Gibson, 2017; Sanderson, Xu, et al., 2017).

For both event attribution and projections of extremes, climate model simulations are widely used as they encapsulate our understanding of how human interference might affect the climate system. Because models exhibit a range of biases (Ehret et al., 2012) including their ability to reproduce the observed frequency distribution of extreme events and/or long-term trends (Angélil et al., 2016; Bellprat & Doblas-Reyes, 2016; Sippel et al., 2016), the accuracy of model-derived statements pertaining to extremes is not always clear. This has been demonstrated in sensitivity studies where attribution results can change in their sign depending on the model, observational data set, or method used. For example, the likelihood of occurrence of specific rainfall extremes can either be found to be more likely (positive attribution statement), less likely (negative statement), or hardly changed (neutral statement) as a consequence of anthropogenic emissions depending on the approach taken (Angélil et al., 2017; Hauser et al., 2017). For temperature extremes, the sign of the attribution statement may not change, but the actual attribution statement in terms of the quantification of how much anthropogenic climate change has altered the likelihood of the event can vary by an order of magnitude (Angélil et al., 2017). Furthermore, model-simulated extremes may be systematically biased across various models compared to observations/reanalyses (Angélil et al., 2016; Bellprat & Doblas-Reyes, 2016; Christensen et al., 2008; Donat et al., 2017; Wang et al., 2014), and therefore, taking the median or mean of the metric of interest across ensemble members can be unreliable (King & Karoly, 2017; King et al., 2017; Lewis & King, 2017; Perkins-Kirkpatrick & Gibson, 2017). Such biases are not necessarily reduced after the poorest performing models have been removed from an ensemble; indeed, this process can reinforce model biases if metrics are not carefully chosen, since the best performing models might have common biases due to shared model development history (so-called model interdependence; Herger et al., 2018).

One way to mitigate some of these issues is to constrain the regional changes in frequency and intensity of hot temperature extremes by the shape of the model's present-day temperature distribution (Borodina et al., 2017). Other studies have developed statistical bias correction schemes, the vast majority focusing on correcting for distribution shapes when they are not representative of the distribution shapes of observational data. Many of these studies involve a procedure in which a "transfer function" is derived by matching percentiles between simulated and observed cumulative distribution functions (sometimes also referred to as *quantile mapping* or *histogram equalization*) and have been expanded on and refined in the last decade (Hempel et al., 2013; Jeon et al., 2016; Li et al., 2010; Piani, Haerter, et al., 2010; Piani, Weedon, et al., 2010; Sippel et al., 2016). The aim of such methods is to also improve *out-of-sample* results (a term used throughout this paper to describe time periods that have not been used to apply bias corrections and will be used to test their effectiveness).

A fundamental issue with most of these bias correction techniques is that they are often applied and tested on the same data ("in-sample") but not in the period of their intended application (for example, because no observational data exist in the later 21st century). There is the risk that while the correction works perfectly in-sample (where observations are available), it may actually degrade predictability out-of-sample. This may be because not all relevant model biases for the metric of interest were considered in the calibration. In statistics, the equivalent might be that when we see success at interpolation, it by no means guarantees success at extrapolation.

A solution is out-of-sample testing using long observational records or model-as-truth experiments, which are common in some areas of climate science (Abramowitz & Bishop, 2015; Herger et al., 2018; Knutti et al., 2017; Sanderson, Wehner, et al., 2017) but appear to be sparse in others such as in the extremes community where they are critically needed. In this study we test one quantile-based bias correction method (Jeon et al., 2016; hereinafter referred to as the *Jeon method*). Their bias correction was applied to the standard event attribution method, which utilizes two model-simulated distributions of weather, each forced under a different climate scenario: a counterfactual "natural" world without industrialization (commonly termed "NAT") and the "real world" forced with all known natural and anthropogenic boundary conditions (commonly termed "ALL" or "RW"). Of the bias correction methods already mentioned (Hempel et al., 2013; Li et al., 2010; Piani, Weedon, et al., 2010, Piani, Haerter , et al., 2010; Sippel et al., 2016), the Jeon method is the most simple. It adjusts the event magnitude that is being attributed, by ensuring its percentile (relative to the simulated distribution) equals the percentile of the observed event (relative to the observed distribution). For example, if the simulated tail is longer than the observed tail (as is the case in their study), the observed event magnitude is shifted further out into the tail until the two percentiles (each relative to their own distributions) are equal. However, such a correction, although perfect in-sample by definition, may not reduce biases out-of-sample, which also depends on the probability of extremes in a world with different forcings. We test for this possibility below.

Apart from testing the out-of-sample skill of the Jeon method, we also detail a new method to correct for biased model distribution shapes in multimodel ensembles. The technique selects the subset of climate simulations from a multimodel ensemble that reduces distribution biases (when compared to a model-as-truth), following the flexible approach introduced in Herger et al. (2018). Here a modeled distribution is obtained by pooling data from a collection of climate models. Similar to previous methods (Hempel et al., 2013; Sippel et al., 2016), it corrects for the entire distribution shape, allowing it to be used for any distribution-based problem of interest, rather than just exceedance probabilities (EPs; which the Jeon method is limited to). The two methods (Jeon and the subset selection approach introduced here) can also be used in combination, providing a third bias correction option. Using long model runs (1870–2100), we test and compare the effectiveness of these three approaches for assessing the probability of extremes in a changing climate, relative to a baseline where no correction is performed. We then compare the relative influence of tail bias on attribution statements versus another relevant source of uncertainty—the bias of response to changes in long-term radiative forcing. Finally, we discuss what type of bias correction and model evaluation strategies should be prioritized to determine whether models are fit for purpose in assessing extremes in a changing climate.

2. Data

We use one Coupled Model Intercomparison Project Phase 5 (CMIP5; Taylor et al., 2012) simulation per modeling institute (21 simulations). The simulations cover the 1870–2100 period (RCP8.5 after 2005) and can be found in Table S1 in the supporting information. We split the 231 years into seven 33-year periods to explore out-of-sample testing. The seven time periods (TPs) are hereinafter referred to as TP1 (1870–1902), TP2 (1903–1935), TP3 (1936–1968), TP4 (1969–2001), TP5 (2002–2034), TP6 (2035–2067), and TP7 (2068–2100). We select time periods covering over 30 years to be able to adequately resolve the statistics of extremes and to reasonably sample modes of (decadal-scale) variability.

One model per institute is chosen from the CMIP5 archive in order to reduce model interdependency. Reducing model interdependency is an important step before performing model-as-truth experiments (see, e.g., Abramowitz & Bishop, 2015, and Sanderson, Wehner, et al., 2017) as it helps avoid artificial skill improvements due to the "truth" model being too similar to the remaining model simulations (increasing the risk of overfitting). Choosing one model per institute removes multiple initial condition members of the same model as well as similar or similarly calibrated models. By doing this the average model-to-model distances are expected to become more similar to the average model-to-observation distances (Herger et al., 2018). Indeed Figure S1a shows that for surface air temperature, the average Kolmogorov-Smirnov (KS) test statistic between these 21 simulations and the land-only gridded observational product CRU-TS, v4.00 (Harris et al., 2014) is generally smaller than the mean model-model KS value. Results for total precipitation (Figure S1b) are similar, with model-obs KS values varying slightly more within the spread of model-model KS values across regions.

Distributions of monthly mean surface air temperature (tas) and total precipitation (pr) are analyzed over 58 WRAF2-v3.0 regions (see Figure 1). The regions are on average $2 \cdot 10^6$ km^2 in size. We apply the Weather Risk Attribution Forecast (WRAF) masks to the model data and calculate area-weighted monthly spatial averages over each region, covering the 231-year period. Note, the analyses could equally be performed on daily data; however, this would reduce the model pool size. This work also primarily serves as a proof of concept, and we thus decided against higher temporal resolution.

No observational products were used in this study, except for in Figure S1. Instead, each model is removed from the ensemble and used as if it were observations, commonly referred to as either model-as-truth experiment or perfect model setup (see section 3.1). With this, we avoid the problem with long observational records having inconsistent quality through time as a consequence of varying station density (Macias-Fauria et al., 2014) yet are still able to test the fidelity of the bias correction approaches.

3. Methods

In this study we define extreme events as the 1-in-1-year and 1-in-5-year return values based on monthly temperature and precipitation data. Even though extremes are often analyzed on a daily time scale, the concept itself can be well demonstrated using 1-in-1-year and 1-in-5-year thresholds using monthly averages as done here. Furthermore, the sensitivity of extremes metrics such as the probability ratio (PR; looked at in this study and discussed later) to the temporal scales of the events (daily, 5-day, and monthly) have already been documented (Angélil et al., 2018). The 1-in-1-year return value is the 91.67th percentile for warm and wet months and the 8.33th percentile for cold months from the distribution of 33 years ($12 \times 33 = 396$ points) in the middle TP (TP4). Note, that this is roughly (but not exactly) the climatology of the locally warmest/coldest/wettest month in the year. The 1-in-5-year return value is the 98.33th percentile for warm and wet months

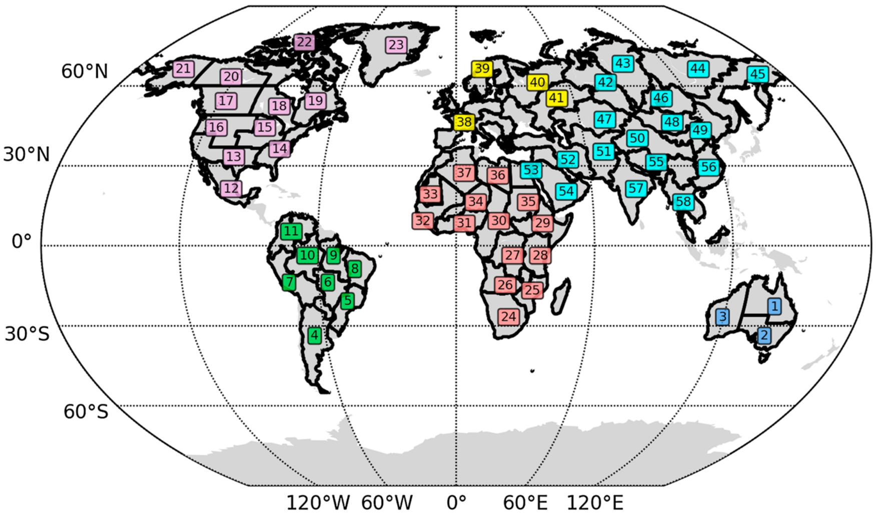

Figure 1. This map shows the 58 WRAF2-v3.0 regions used in this study. Each region is roughly 2·10^6 km^2 on average. The regions are color-coded according to their continents.

and the 1.67th percentile for cold months. Given that results for 1-in-1-year events are "cleaner" than those for 1-in-5-year events (for the latter, EPs of 0 were frequent enough to render results indistinguishable between some TPs), and since key findings are similar between both, results for 1-in-5-year extremes are shown in the supporting information. Results for 1-in-1-year and 1-in-5-year wet months are also only shown in the supporting information.

3.1. Models-as-Truth Experiment

Model-as-truth experiments as conducted in this study involve removing one of the ensemble members and treating it as if it were observations or "truth." The remaining ensemble is then calibrated (using either the Jeon method or the subset selection method introduced in section 3.3) to try to better estimate the truth member, using data from the middle TP (TP4). The calibrated ensemble can then be tested out-of-sample in the remaining six TPs against the truth member. The ability of each technique to offer an improvement over the default ensemble (the 20 remaining ensemble members) is then assessed. The process is repeated with each of the 21 models playing the role as truth, and results are aggregated to provide an uncertainty estimate of the ability of each bias correction approach. As mentioned in section 2 above, before conducting model-as-truth experiments we make sure that the model-model distances within our ensemble are at least that of model-observation distances. This gives us some confidence that success in model-as-truth experiments should translate to effective application of these techniques when making predictions out-of-sample. Note, however, that passing model-as-truth experiments is a necessary but not sufficient test for real out-of-sample skill. The reason being that no observations are involved, and the model ensemble is solely an approximation to the real-world application.

3.2. Jeon Method

As briefly mentioned in the introduction, the Jeon method (Jeon et al., 2016) accounts for the discrepancy between the probabilities of extreme weather events derived from the truth and the model data set by mapping the truth quantile to the modeled quantile. We then calculate temperature and precipitation thresholds in the model-as-truth and remaining 20 model data sets in TP4 (simply using the same percentile in the truth and model distributions to define thresholds is the essence of the Jeon method), rotating through each of the 21 models as truth and for each region separately.

For a real application, we usually start with an observed event that can be described as a certain percentile of the observational record. Here, however, we start with a given percentile (e.g., 91.67th percentile for warm events or 8.33th percentile for cold events) and calculate a model-derived threshold using that percentile. EPs (for warm or wet events) or probabilities of falling below (PsFB; for cold events) are computed relative to this threshold. When applying the Jeon method, the threshold is obtained from the pooled model distribution rather than from the model-as-truth. For a graphical representation of the Jeon method we refer to Figure 3 in their paper.

3.3. Ensemble-Based Subset-Selection Method

In Herger et al. (2018), an optimal subset of model runs is chosen to minimize the root-mean-square error of global temperature or precipitation fields between a truth (either observational product or model-as-truth) and an ensemble average for a given subset size. Here we tailor the method to extremes by finding the optimal subset of CMIP5 model runs that when pooled (i.e., not averaging but rather concatenating all the data into one long vector) minimizes the two-sample KS (Stephens, 1970) test statistic compared to a given truth (model-as-truth in this study). Different to the subset selection in Herger et al. (2018), here we are pooling rather than averaging model runs and we are minimizing the KS test statistic for temperature and rainfall distributions over regions rather than the global root-mean-square error.

We also note that the meaning of “optimal” is not general and can vary depending on the specific application. When we refer to an optimal subset we are talking about the subset that minimizes the cost function for a specific variable, region, TP, model-as-truth, metric, and so on. A globally optimal subset does not exist and would not be very meaningful.

The KS test statistic is defined as the maximum vertical distance between the true empirical survival functions (ESFs) and the ESF of the pooled model runs. The maximum vertical distance is the same as the maximum vertical distance between two empirical cumulative distribution functions (ECDFs; ECDF = 1− ESF). Examples of ESFs are shown in Figure 3. Since there can be any number of members (between 1 and 20) in the optimal subset, we use K to denote the number of pooled model runs found to minimize the KS test statistic.

We note that the Anderson-Darling (Anderson & Darling, 1970) test presents an alternative metric that is more sensitive to the tails of distributions than the KS test (Heo et al., 2013). We attempted to select a subset to minimize the Anderson-Darling test statistic; however, the optimization was not feasible due to computational constraints, given the more complex cost function that had to be rewritten for the mathematical solver.

A workflow of the novel methodology is shown in Figure 2, illustrated for one particular region and one model-as-truth. The same procedure is then repeated for the remaining WRAF regions and models as truth.

As noted above, the optimal subset is only calculated using TP4. Each implementation of the optimization approach finds an optimal subset for a given ensemble size K, so in addition to selecting an optimal subset, we need a mechanism to choose the ensemble size best suited across different TPs. To do this, we use a cross-validation (CV) approach using the middle three 33-year TPs (TP3–TP5). We optimally select ensemble members for all ensemble sizes using one of these TPs and test the skill of these optimal ensembles on the other two periods. This process is repeated for all three TPs and results averaged to find the best out-of-sample cross-validated optimal subset size K_{CV}—see Figure 2. We refer to the period we train on (that is, derive the optimal ensemble) as in-sample and the periods we test on—periods never seen by the subset-selection algorithm—as out-of-sample. The advantage of this approach is of course that we have models as truth both in-sample and out-of-sample, and we can thus test the degree to which our bias correction methods degrade out-of-sample. We can also go much further out-of-sample had we just relied on long observational records. We use the term *optimal ensembles* to denote the ensembles that are selected for a given ensemble size. *Optimal subset* is used for the overall best (lowest KS test statistic) subset across all ensemble sizes.

Consider case 1 in Figure 2 (red rectangle), where we train on TP4 and test on TP3 and TP5. For each ensemble size between 1 (single best simulation) and 20 (all runs pooled), we find the subset of ensemble runs, which when pooled minimize the KS test statistic in the in-sample period (TP4) compared to the model-as-truth—see ECDF inset Figure 2a. This is a nontrivial task as there are, for example, 184,756 possible ensembles of size 10. Due to time-constraint issues, a “brute force” approach is therefore simply not possible for each model-as-truth, over each of the 58 regions, for three TPs, and two variables. Instead, we use the state-of-the-art mathematical programming solver Gurobi (Gurobi Optimization, Inc. 2015) to minimize the KS test statistic for a given ensemble size. Details, including a link to a simplified Python script used to do this can be found in the supporting information. Note that Gurobi is only ever used to obtain the optimal ensembles in the training periods. We end up with a curve similar to the schematic in Figure 2a: the KS test statistic of the optimal ensemble as a function of ensemble size. Note that the KS test statistic can vary between 0 and 1. Here $K_{\mathrm{train,TP4}}$ is the number of simulations in the optimal subset for TP4.

Using only $K_{\mathrm{train,TP4}}$ to go out-of-sample may be risky, as we do not know if the members of this optimal subset are still optimal in the two testing periods when climate forcing is different. It is possible that a different value of K would be best out-of-sample. The next step in the process is therefore to use the in-sample ensembles

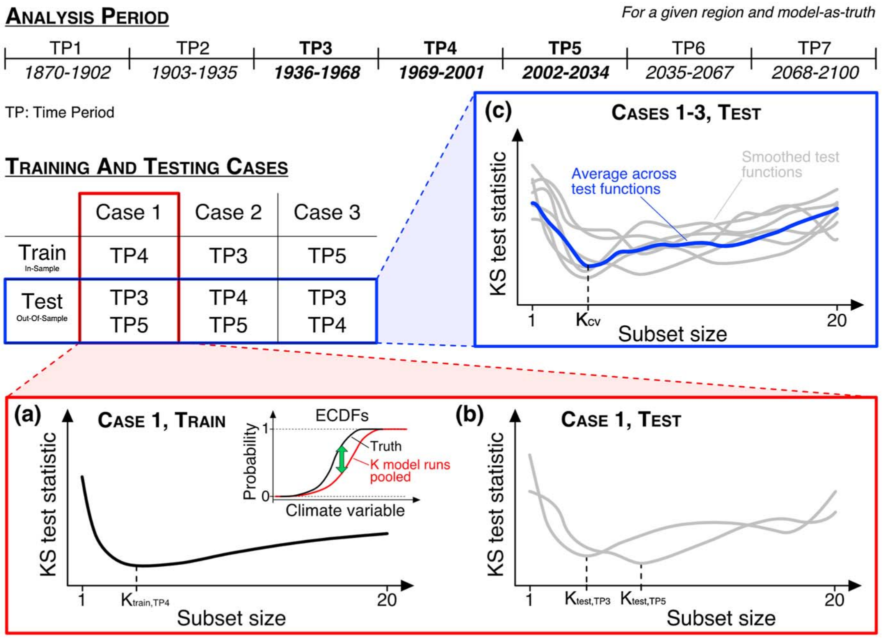

	Case 1	Case 2	Case 3
Train In-Sample	TP4	TP3	TP5
Test Out-Of-Sample	TP3 TP5	TP4 TP5	TP3 TP4

Figure 2. Methodological workflow of the study. The analysis period is split into seven 33-year periods (TP1–TP7). Only TP3–TP5 are used to obtain the cross-validated optimal subset size. (a) For a given model-as-truth (could equally be observations in practice), we obtain the optimal ensembles in the training set (case 1) for subset sizes 1–20. Those ensembles are then tested out-of-sample (in TP3 and TP5), see (b). Performance of the optimal ensembles are tested out-of-sample in a total of six test periods (gray lines in blue box c). To account for noise generally at small ensemble sizes, these functions are smoothed using a running mean of three ensemble sizes. To obtain the cross-validated optimal subset size (K_{CV}), we average across all six smoothed test cases (blue line in c). The subset size at the minimum of this function for a particular region and model-as-truth is then used for the remainder of this study. A different size is obtained depending on the chosen region and model-as-truth. ESDFs = empirical cumulative distribution functions; KS = Kolmogorov-Smirnov.

for each K found in Figure 2a to calculate the KS test statistics in the two out-of-sample periods (see Figure 2b). Those KS values will likely be higher than the in-sample values. For each TP that we test on out-of-sample, we obtain a slightly different curve. Ideally, we want the K with the minimum KS value for those curves ($K_{\text{test,TP3}}$ and $K_{\text{test,TP5}}$) to be close to the K with the minimum KS value found in-sample ($K_{\text{train,TP4}}$), but this is not always the case. To avoid overfitting we search for the optimal K across all three cases (termed CV in the literature).

We repeat the steps described above for cases 2 and 3, where the training and testing periods are changed. The curves for the six out-of-sample tests are shown in Figure 2c. Gray curves illustrate the smoothed functions using a moving window that averages the KS test statistics across three ensemble sizes. The reason we smooth those curves is because the gray lines can be very noisy at small ensemble sizes. Failure to address this might lead to overfitting in an ensemble subset size that is small.

Next, we average across the six gray curves to obtain the blue one. The cross-validated ensemble size, K_{CV}—the size used for the remainder of the study (for a given region and model-as-truth), is the subset size with the overall smallest KS test statistic across these six out-of-sample tests. We refer to it as *cross-validated optimal subset size*. An example of in-sample and out-of-sample KS values for WRAF region 38, the Southern European Economic Area (EEA), and CSIRO-Mk3.6.0 r2i1p1 as the truth, can be found in the supporting information (Figures S3 and S4). This is an example where it is particularly important to execute the smoothing step. Without it we would end up with a small subset size, where the curves are noisy. For this region, we end up with a K_{CV} subset size larger than the in-sample optimal subset sizes. The optimal ensemble in TP4 for K_{CV} then becomes the cross-validated optimal subset. A larger ensemble size means that we are relying on a wide range of climate models rather than betting on a small subset of models to perform well out-of-sample. Note that TP3 and TP5 may now not be considered as truly out-of-sample for testing the ability of our bias correction approaches, since they are used to find the optimal cross-validated subset size K (this is why they are in boldface in Figure 2).

The pooling of model runs from the CMIP5 archive for each 33-year period mitigates the effect of internal variability (each run being in a different state of internal variability). What remains is therefore primarily the forced response, being the main difference between the TPs.

3.4. Calculation of Extremes Metrics

After correcting for shape bias, whether it be with the Jeon or subselection approach, we calculate EPs (for warm and wet events), PsFB (for cold events), and PRs — the ratio of two EPs or PsFB characterizing the change in probability of the event between two periods of different forcings, in TP1 – TP3 and TP5 – TP7.

The PR is typically used by the event attribution community between ALL- and NAT-forced climates to characterize the anthropogenic contribution to the chance of an extreme but is unconventionally used in this study between two 33-year periods within the 1870 – 2100 period. This allows out-of-sample testing forward and backward in time and so includes a broader range of forcing changes with which to test the bias correction techniques. The EPs, PsFB, and PRs obtained from the reference distribution of all 20 models pooled when using the truth to define the threshold (in TP4) are shown against EPs, PsFB, and PRs (again in the distribution of all 20 models pooled) obtained when using the Jeon method to calculate the threshold (light and dark green markers in Figures 5 and 6). The same procedure is also applied to the cross-validated optimal subset (yellow and orange markers in Figures 5 and 6). The skill of both methods is gauged by comparing them to the true EPs, PsFB, and PRs derived from using each model-as-truth.

4. Results

4.1. Obtaining the Cross-Validated Optimal Subset

Cross-validated optimal subsets for each of the 58 WRAF regions are obtained as described in section 3.3. Here we illustrate the ensemble-based subset-selection method in TP4 using WRAF region 38, which is the Southern EEA. ESFs and normalized histograms are shown in Figure 3. The truth (CSIRO-Mk3.6.0, r2i1p1) is shown in black and the remaining 20 CMIP5 simulations in gray. The model run closest to the truth in terms of the KS test statistic is shown in cyan. Note that the warm tails of most of the CMIP5 runs are too short relative to the truth. This tail bias persists in other TPs (seen in Figure 5a and discussed later). The ESFs for precipitation are shown in Figure S2.

Simply pooling all 20 model runs will not solve this problem, as shown with the light green line. This is where the subset-selection comes into play. The red line is the optimal subset in the in-sample period (here: TP4), with $K = 7$. The cross-validated optimal subset is shown in yellow, with $K_{\mathrm{CV}} = 9$. Both the red and yellow lines are closer to the observations than the green line. Note, that any subset selection approach can only be successful if the original ensemble spans the entire distribution of the true conditions, as it does in this case.

The horizontal dashed lines show the 1-in-1-year warm and cold month events (91.67th and 8.33th percentiles, respectively). The vertical lines refer to the corresponding thresholds of the different distributions. The thresholds for the optimal subset and cross-validated optimal subset are now positioned closer to the true thresholds, which is not guaranteed in all cases since we are optimizing for the shape of the entire distribution not specifically the tails. Thresholds for the "20 runs pooled" distribution (light green) and the cross-validated optimal subset (yellow) are later used for the Jeon method.

Figure 4a confirms that the subselection is working in-sample (TP4) for all regions, showing the in-sample KS test statistic values based on absolute surface temperature. The marker colors are consistent with what was used in Figure 3. Region 38 is highlighted in gray as this is the region used to illustrate results in Figure 4b and subsequent panels. The smaller the KS test statistic, the closer the corresponding distribution is to the truth. There are even some regions where all the model distributions are significantly different ($p < 0.05$) from the true distribution (black border around markers).

We observe that simply pooling all 20 available model runs (green marker) already seems to bring the distribution closer to the truth. It is usually better than most individual model runs. However, choosing ensemble members optimally can improve our pooled distribution even further. As before, the red marker is the subset that is optimal in-sample (here: TP4), and the yellow marker is the optimal subset in TP4 for size K chosen across TP3 – TP5. Results for precipitation are similar (Figure S5a).

The cross-validated optimal subset size is usually larger than the in-sample subset size (not shown). This tendency toward larger ensemble sizes is consistent with findings by Reifen and Toumi (2009) who suggest

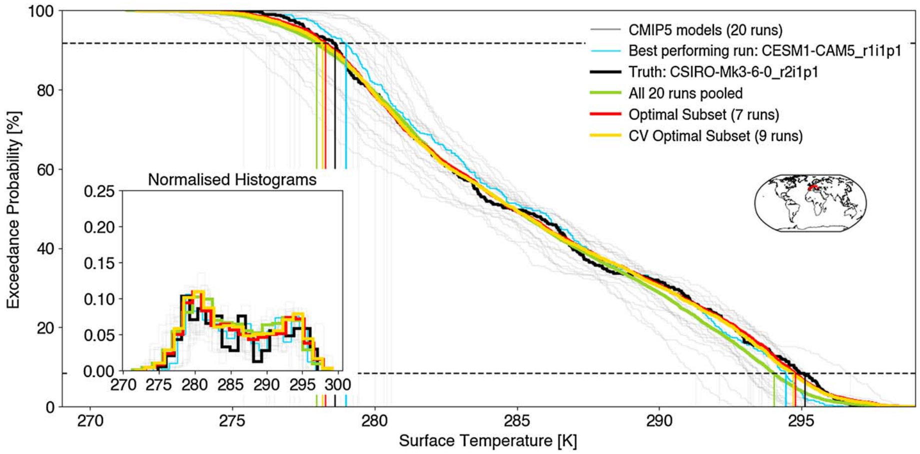

Figure 3. Empirical survival function of monthly surface temperature in period TP4 over WRAF region 38 (Southern European Economic Area) for CSIRO-Mk3.6.0 r2i1p1 as truth. The raw (no correction for mean bias) individual Coupled Model Intercomparison Project Phase 5 (CMIP5) model distributions are shown in gray, and the truth in black, each distribution consisting of 396 (33 years × 12 months) points. The cyan curve is the single best performing run (in terms of the lowest Kolmogorov-Smirnov test statistic compared to the model-as-truth). The green curve is the 20 CMIP5 runs pooled. The red curve is the optimal subset of CMIP5 runs, which results in the lowest KS test statistic compared to the truth derived within TP4 (happens to be $K = 7$), and the yellow curve is the optimal subset when $K = 9$, being the subset size best suited across TP3–TP5 (tuned via cross-validation). Vertical lines show the 1-in-1-year cold (8.33th percentile) and warm (91.67th percentile) thresholds derived from the various distributions. CV = cross-validated.

that having a “portfolio” of climate models is better than relying on a small subset when making predictions as there is a risk associated with small ensemble sizes.

In Figure 4b, which shows results only for WRAF region 38, we test whether the subset selection improves skill, measured as the KS test statistic, in the remaining six TPs. Here each model is used as the truth, so there are 21 points in each of the boxplots. By definition, the bias correction improves skill in-sample (TP4) relative to the case where no correction is performed (all runs pooled). We note that it also improves skill out-of-sample as far as TP1 and TP7 (biases in the shape tend to persist), although the skill gradually diminishes (yellow and red boxplots form a V shape) the further away in time (and forcing) we move from the training period. Results in this format for the other 57 regions are similar (not shown here), as well as for precipitation (Figure S5b). Given that skill of the optimal subset and cross-validated optimal subset are fairly similar, we only show results using the cross-validated optimal subset in the remainder of the study.

4.2. Application of Bias Correction to Extremes

Now that we have confirmed that the ensemble-based subset-selection successfully improves the shape of the distribution in-sample and out-of-sample, we can focus our attention on extreme events. We start with EPs and PsFB (section 4.2.1) for warm and cold events respectively before we test its skill on PRs (section 4.2.2). For extremes, we are of course only interested in the tails of the distribution even though we calibrated the whole distribution to be similar to the truth. However, calibrating on the whole distribution still makes sense as we are not fixing usage to a particular extreme and can thus explore a range of thresholds for extremes in a consistent way. Moreover, we ensure that the mean climate (i.e., the bulk of the distribution) is right and avoid an unrealistically truncated distribution (by, e.g., solely optimizing the tail of the distribution).

4.2.1. Probabilities of Exceeding or Falling Below a Threshold

Calibrating on the shape of the distribution in-sample does not guarantee that we subsequently get better estimates of PsFB or EPs. This is an assumption of *metric transitivity*, meaning that we expect an improvement in one metric—the shape of the distribution, to increase skill of another metric—EPs or PsFB—as though they were dependent. If this were not the case, testing the metric out-of-sample on anything other then what it was calibrated on in-sample would likely give poor results. In this section we test if metric transitivity holds for temperature extremes. Results for wet events can be found in the supporting information.

Figures 5a and 5b show the probabilities of exceeding the 91.67th percentile in TP4 (1-in-1-year warm events; left column) or falling below the 8.33th percentile in TP4 (1-in-1-year cold events; right column) over Southern EEA using CSIRO-Mk3.6.0 as the truth. Results for 1-in-5-year warm and cold month events are shown

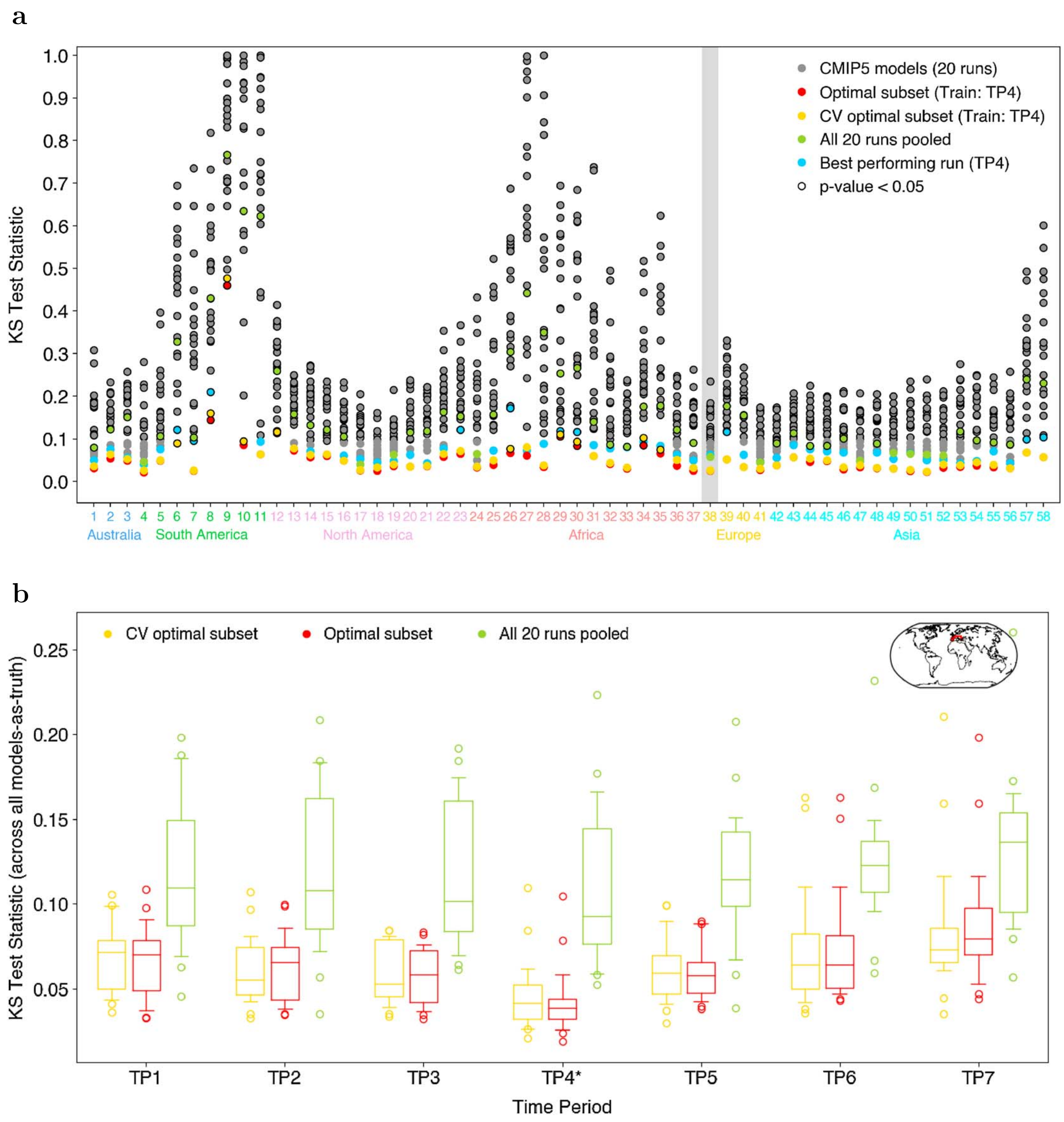

Figure 4. (a) The in-sample Kolmogorov-Smirnov (KS; TP4) test statistics for all WRAF regions are shown based on CSIRO-Mk3.6.0 r2i1p1 as truth. TP4 is used as our training period, and the KS test statistics (compared to the model-as-truth) of the individual and pooled runs are shown within the same period. We show results of absolute surface temperature from the individual CMIP5 simulations (gray), the single best run (cyan), all 20 runs pooled (green), the optimal subset (red), and the cross-validated optimal subset (yellow). Markers have a black border if the corresponding distribution is significantly different ($p < 0.05$) from the distribution of the truth. WRAF region 38 (Southern European Economic Area) is highlighted in gray. (b) Results for WRAF region 38 are aggregated across all models as truth and for the seven time periods (TPs). In all cases, the subset is obtained in TP4 and applied to the other time periods. Boxplots for the optimal subset (red), cross-validated (CV) optimal subset (yellow), and all 20 runs pooled (green) are shown. For the boxplots, the centerline is the median, the box spans the 25th–75th percentile range, and the whiskers span the 10th–90th percentile range. CMIP5 = Coupled Model Intercomparison Project Phase 5.

in Figure S6. We see that the probability of warm events decreases toward earlier TPs and increases toward later TPs (vise versa for cold events). We do not see such clear changes in EPs for precipitation (Figure S7a for 1-in-1-year events and Figure S8a for 1-in-5-year wet month events). For warm events, the increase in EPs toward TP7 is significantly larger than the decrease in EPs toward TP1, indicating the stronger change in forcing toward the end of the 21st century. There are two additional markers compared to Figure 4. Dark green markers refer to the case when all 20 runs are pooled and the threshold was based on this pooled distribution in TP4 (Jeon method) rather than the truth distribution. Orange markers refer to the cross-validated optimal

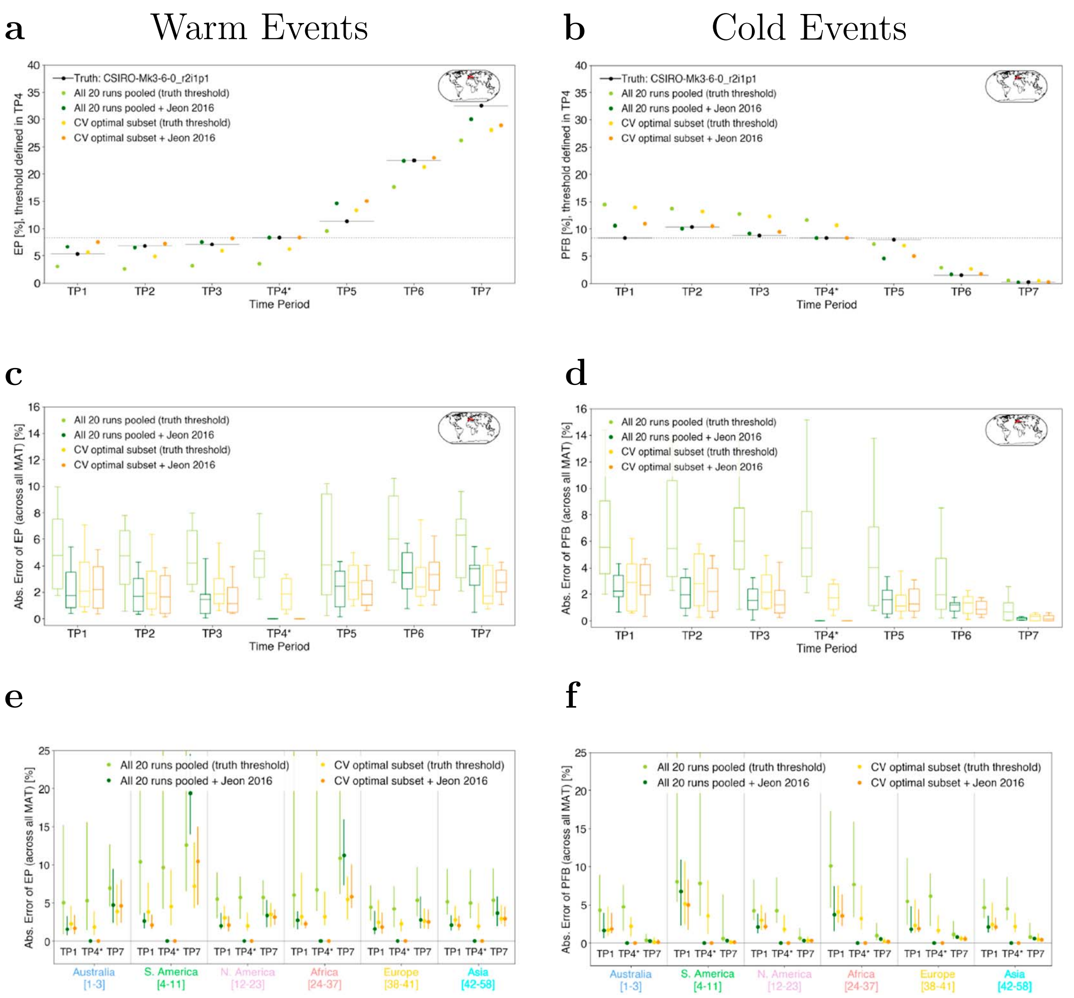

Figure 5. Exceedance probabilities (EPs) for 1-in-1-year warm month thresholds are shown in the left column and PsFB for 1-in-1-year cold month thresholds are shown in the right column. (a) EPs for CSIRO-Mk3.6.0 r2i1p1 as truth and WRAF region 38 (Southern European Economic Area) are shown for TP1–TP7. The threshold is defined in TP4 and its EP is plotted for the remaining time periods (TPs). EPs of the truth (black dot and line) are compared to the distribution of all 20 runs pooled without (light green dot) and with applying the Jeon method (dark green), and the cross-validated (CV) optimal subset without (yellow) and with applying the Jeon method (orange). (b) is the same as (a) but for cold events. (c) For the same WRAF region 38, we aggregate absolute errors of EP across all models as truth. The errors are obtained by calculating the absolute distances between the truth and the remaining ensembles. For the boxplots, the centerline is the median, the box spans the 25th–75th percentile range, and the whiskers span the 10th–90th percentile range. (d) is the same as (c) but for cold events. (e) aggregates the results shown in (c) across six continents by averaging results within those continents. Absolute errors of EP in TP1, TP4, and TP7 are shown. The lines span from the 10th to the 90th percentile, and the dot indicates the median. Panel (f) is the same as (e) but for cold events. MAT = model-as-truth.

subset with threshold derived from this subset itself in TP4 (again Jeon method) rather than the truth. The closer the colored markers are to the truth (black marker with horizontal line) outside of TP4, the more skillful the given bias correction procedure. Both the Jeon and subset selection methods appear to improve EPs and PsFB relative to when no correction is performed (light green marker).

Figures 5c and 5d show the absolute error between each of the colored markers and the truth, still over Southern EEA, using each model-as-truth, allowing us to present a range of skill. By definition, the absolute error for the methods based on the Jeon method are 0 in the in-sample period (TP4). Again, we observe that both methods improve EPs and PsFB as far from the training period as TP1 and TP7. Both methods also improve skill in the EP for precipitation events going back to TP1 and forward to TP7 (Figures S7b and S8b). The significant reduction in the size of the absolute error in Figure 5d toward the end of the 21st century is due to the reduction in the probabilities of cold extremes in a rapidly warming climate.

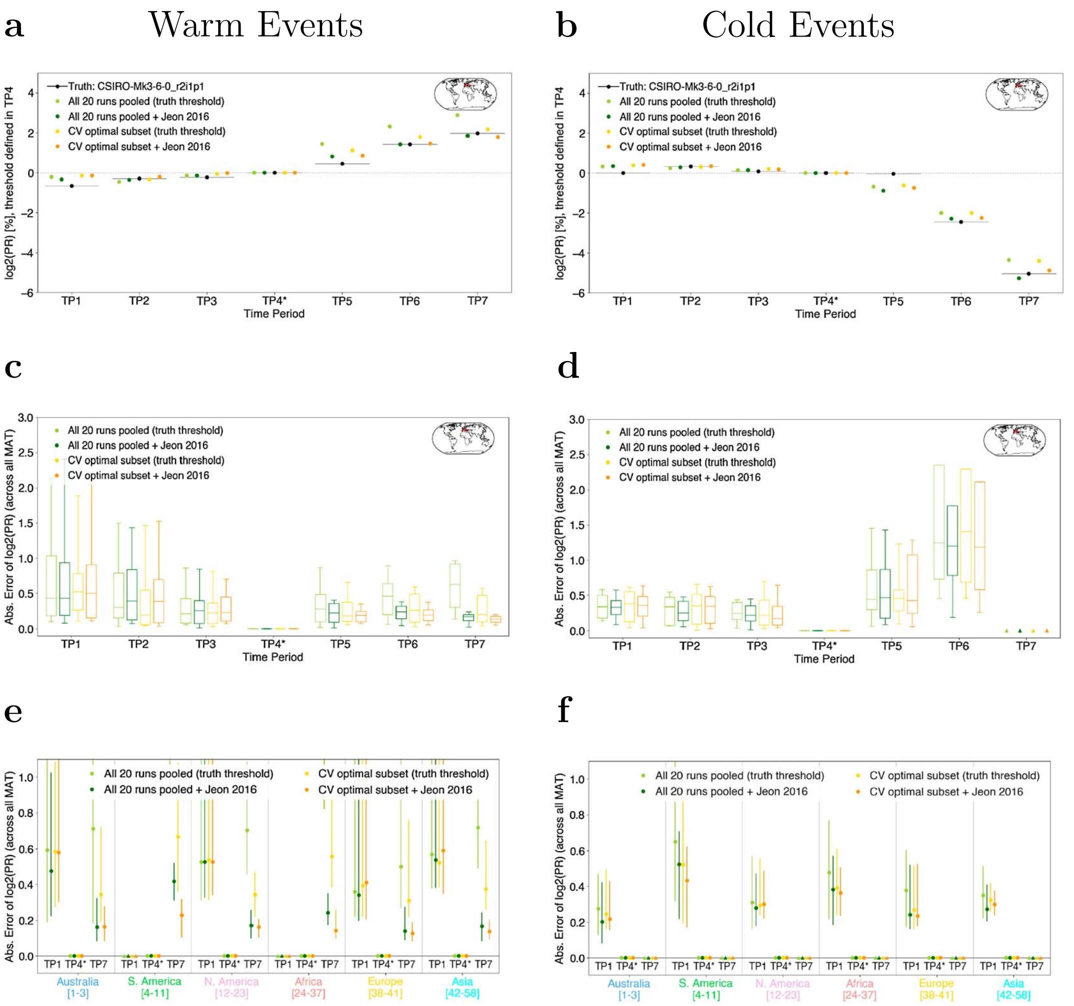

Figure 6. Probability ratios (PRs) for 1-in-1-year warm months are shown in the left column and for 1-in-1-year cold months in the right column. The threshold is defined in TP4. (a) log2(PRs) for CSIRO-Mk3.6.0 r2i1p1 as truth and WRAF region 38 (Southern European Economic Area) are shown for TP1 – TP7. The probability ratio (PR) in time period (TP) *x* is defined as PRx = EP(TPx)/EP(TP4). PRs of the truth (black dot and line) are compared to the PRs of all 20 runs pooled without (light green dot) and with applying the Jeon method (dark green); the cross-validated (CV) optimal subset without (yellow) and with applying the Jeon method (orange). Panel (b) is the same as (a) but for cold events. (c) For the same WRAF region 38, we aggregate absolute errors of log2(PR) across all models as truth. The errors are obtained by calculating the absolute distances between the truth and the remaining ensembles. For the boxplots, the centerline is the median, the box spans the 25th – 75th percentile range, and the whiskers span the 10th – 90th percentile range. Panel (d) is the same as (c) but for cold events. Panel (e) aggregates the results shown in (c) across six continents by averaging results within those continents. Absolute errors of log2(PR) in TP1, TP4, and TP7 are shown. The lines span from the 10th to the 90th percentile and the dot indicates the median. The arrow-up markers indicate that at least four out of 21 values for a given TP and continent are infinity. Panel (f) is the same as (e) but for cold events.

Figures 5e and 5f show results averaged within the six continents: Absolute errors for each model-as-truth are averaged across all WRAF regions that fall within a given continent. We summarize results by only showing results for TP1, TP4 (in-sample), and TP7 for a given continent. As for the Southern EEA, the bias correction strategies generally improve skill out-of-sample. The exception being the Jeon method in TP7 over South America and Africa for warm events (Figure 5e), where the absolute error of the dark green marker is higher than for the light green marker. Applying the Jeon method on top of optimally selecting ensemble members usually leads to marginal improvements in skill beyond only optimally selecting ensembles members. Similar conclusions can be made for precipitation (Figures S7c and S8c) and 1-in-5-year temperature events (Figure S6c).

So calibrating on the shape of the distribution leads to improved EPs and PsFB, even when training and testing periods are several decades apart. These findings are consistent with a study by Borodina et al. (2017), who found a strong correlation between the modeled present-day temperature distribution and the projected frequency of warm extremes (defined as future exceedance of today's 95th percentile), which they then use to constrain changes in the intensity of warm extremes in various regions. The reason the Jeon method and our subset selection method are successful (relative to no bias correction) is because shape bias tends to persist through time, as already mentioned, and EPs are strongly influenced by the shapes of the tails, which can be strikingly biased in many cases. Although EPs improve substantially with the bias correction methods, they are still imperfect; one reason is likely another model bias, which is discussed next.

4.2.2. Probability Ratios

In the event attribution community, it is not the EP or PFB but rather the PR that is of interest, being the ratio of two EPs or PsFB, typically between NAT- and ALL-forced simulations. The NAT scenario would refer to the same TP but under a forcing scenario representative of a world without anthropogenic influences. However, here the PR is calculated by dividing the EP or PFB in each TP, by the EP or PFB in TP4 (PRx = EP(TPx)/EP(TP4)). In Figure 6 (same as Figure 5 but for PRs) we test the effectiveness of the different bias correction strategies on the PR by comparing the ratio of two EPs (warm events; left column) or PsFB (cold events; right column) in the bias corrected distributions against the true PR. Results for 1-in-5-year warm and cold month events are shown in Figure S9.

Figure 6a, over Southern EEA using CSIRO-Mk3.6.0 as the truth, indicates that the EP in TP1 – TP3 is lower than in TP4 (PR < 1; log2(PR) < 0); and the EP in TP5 – TP7 is higher than in TP4 (log2(PR) > 0), when defining the threshold in TP4. The bias correction strategies appear to help as we move toward TP7: dark green, yellow, and orange markers lie closer to the black marker than the light green marker does. However, the bias correction methods do not appear to help going back to TP1, which can be considered most similar to what would be done in event attribution. In Figure 6b, we see that cold events in TP1 – TP3 are more common than in TP4 (log2(PR) > 0) and cold events in TP5 – TP7 are much less common than in TP4 (log2(PR) < 0). It appears (going back to TP1 or forward to TP7) that the bias correction strategies hardly help.

Figures 6c and 6d provide more complete results for Southern EEA, as they show the spread when using each model-as-truth (each boxplot consisting of 21 points). Arrow-up markers in Figure 6d indicate PRs of infinity as cold events defined in TP4 never occur in TP7 where the forcing conditions are very different. Again, we see that it is only for warm events going into the future that the Jeon and subset selection methods help, which is even more apparent for 1-in-5-year warm events (Figure S9c). The reason for this is most likely because warm events are very well sampled as we move toward TP7; far more than cold events going toward TP7 or warm events going back to TP1 (both of which decrease in likelihood). Even though cold events going back to TP1 increase in likelihood, the effect of the Jeon and subset selection methods is not as strong as for warm events as we move to TP7; the reason being that anthropogenic climate change is nonlinear. Therefore, for warm events going forward, we are essentially no longer in the tails but rapidly moving toward the center of the distribution, increasing the importance of the shape of the distribution, which we have optimized for. Error in the PR becomes increasingly larger for warm events as we move back to TP1 (similar to what is done in event attribution), or cold events as we move to TP7, since the events become poorly sampled. Therefore, correcting for the shape of the distribution does not appear to improve skill in the PR, allowing for the influence of another bias (long-term regional temperature response to changing CO_2 concentrations) to begin to dominate (discussed later).

Figures 6e and 6f reinforce that what we found for Southern EEA is valid over other regions too: The bias correction methods mostly improve skill in the PR for warm events as we move toward TP7. There also appears to be a noticeable improvement in the skill of the PR for cold events going back to TP1. This finding is consistent with our reasoning discussed in the previous paragraph: As for warm events going toward TP7, cold events going back to TP1 become more frequently sampled, increasing the importance of the shape of the distribution as opposed to just the poorly sampled tails. Arrow-up markers in Figures 6e and 6f indicate errors of infinity. The effectiveness of the bias correction approaches on the PR for precipitation vary depending on the continent (Figure S10c for 1-in-1-year events and Figure S11c for 1-in-5-year events).

4.3. Testing the Relative Importance of Trend and Shape Bias on the PR

To test if the PR is more sensitive to the trend or the shape of the distribution, we use a toy model experiment shown in Figure 7. Using Gaussian distributions, we calculate PRs with different shapes of the distribution

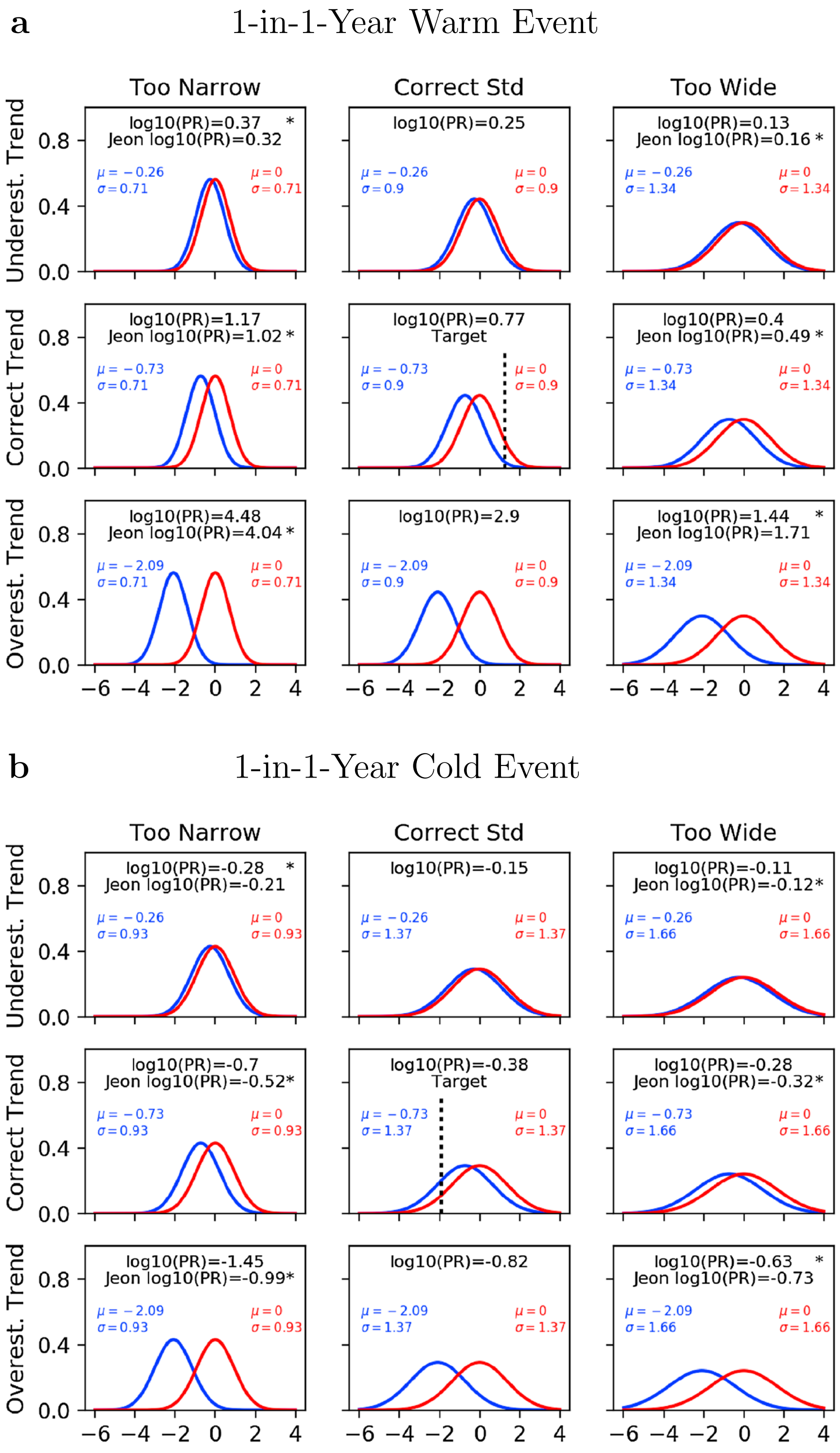

Figure 7. (a) Toy model experiments to demonstrate the relative importance of biases in the shape of the distribution and biases in the trend when calculating the probability ratio (PR). Location (μ) and shape (σ) for the Gaussian distributions were derived from 21 Coupled Model Intercomparison Project Phase 5 simulations for WRAF region 38 (Southern European Economic Area). The red distributions represent the ALL forcing world, and the blue distributions represent the NAT world. The 1-in-1-year warm month (91.67th percentile) of the ALL distribution in the middle panel was used as a threshold for calculating the PR. When applying the Jeon method (relevant only when distribution shapes are too narrow or too wide), the threshold is defined from each "too narrow" or "too wide" ALL distribution. The asterisk indicates which of the two PR estimates is closer to the target PR (middle panel). Panel (b) is the same as panel (a) but for 1-in-1-year cold month events (8.33th percentile).

(figure columns: too narrow, correct, and too wide) and different trends (figure rows: underestimated, correct, and overestimated). Red represents the ALL world and blue the NAT world. To illustrate the idea, we use a 1-in-1-year warm month (91.67th percentile; see black dashed line in center panel) event threshold in panel (a) and a 1-in-1-year cold month (8.33th percentile) event threshold in panel (b) for the calculation of the PR. Results for 1-in-5-year warm and cold month events are shown in the supporting information (Figure S13).

The standard deviation (σ) and location (μ) of these distributions are derived from the same 21 CMIP5 simulations as used for the previous figures, for WRAF region 38 (Southern EEA). Standard deviations for each run are calculated based on monthly mean surface temperature data in TP4 (January averages for cold events and July averages for warm events). The regional temperature response to changing CO_2 concentrations (and thus location difference between the red and blue distributions) was derived by regressing the regional annual average surface temperature against global annual CO_2 concentrations from 1870–2001 (TP1–TP4). We then obtain estimates of "too narrow"/"too wide" and "underestimated trend"/"overestimated trend" by using the 5th and 95th percentiles of distributions consisting of 21 standard deviations or trends (one value per model simulation in each of the distributions). The 50th percentile was used as our target (middle panel in both Figures 7a and 7b). The difference in CO_2 between a natural world (280 ppm) and a recently observed world in 2015 (400 ppm) is 120 ppm. We therefore multiply the slope of the regression by 120 to approximate the temperature change between the NAT and ALL distributions. Note that we make the assumption that we only observe a shift in the mean and the distributions remain Gaussian. Results for a low-latitude region (region 27; the Democratic Republic of Congo) with lower internal variability are similar and are shown in the supporting information (Figure S12).

In addition to the traditional calculation of the PR, being the probability of exceeding the event threshold in the ALL scenario divided by the probability of exceeding the event threshold in the NAT scenario (first line of text within each panel in Figure 7), we obtain PR estimates using the Jeon method (second line within each panel). The asterisk indicates which of the two PR estimates is closer to the target PR ($10^{0.77}$ for the warm extreme and $10^{-0.38}$ for the cold extreme). Correcting for tail bias, for example, with the Jeon method, does not always lead to an improved PR estimate.

As mentioned in section 4.2.2, we hypothesize that the reason we hardly see an improvement in skill when calculating the PR for warm events is because the bias correction strategies only consider biases in the shapes of the distributions, without consideration of other biases such as response bias; for example, how sensitive is the regional long-term temperature to changes in global CO_2 concentrations?

In this toy model setup, the effect of response bias on the PR is roughly the same as that of shape bias for cold events. But for warm events, the effect of response bias is at least an order of magnitude larger than the effect of shape bias: Given a correct trend, the PR varies from $10^{0.4}$ for too wide distributions to $10^{1.17}$ for too narrow distributions (factor of 6; $10^{1.17-0.4}$). However, given a correct standard deviation, the PR varies from $10^{0.25}$ for an "underestimated trend" to $10^{2.9}$ for an "overestimated trend" (factor of 447). For 1-in-5-year warm month extremes the PR changes by a factor of 11 when keeping the trend correct and by a factor of 1,820 for a correct distribution width. So the importance of response bias relative to shape bias increases the rarer the event.

When the standard deviation is underestimated, the sensitivity to the trend is further increased, resulting in a difference of 4 orders of magnitude between underestimated trend and overestimated trend. The toy model therefore suggests that narrower distributions exacerbate the influence of trend bias on the PR and vice versa for overestimated standard deviations. This is because the ratio of the anthropogenic warming signal to the noise of natural variability increases or decreases as the width of the distribution decreases or increases, respectively (Angélil et al., 2018).

5. Discussion and Conclusions

This study examines two bias correction approaches that account for biases in the shape of distributions of surface air temperature and total precipitation. The Jeon method artificially adjusts the threshold in the model distribution to match the percentiles in the true distribution. It is thus a purely statistical method that could result in unphysical multivariate results. As an approach that optimizes for the whole distribution shape, we introduce a novel subset-selection method that optimally chooses ensemble members that when pooled have a distribution most similar to observations or a target truth simulation. Contrary to the Jeon method, the potential applicability of this approach is wider as it optimizes for the entire distribution and also it does not violate the models' physics or multivariate relationships. Apart from risk ratios, it may therefore also be suitable for impact studies and multivariate analyses. Overall results based on the Jeon method were found to be quite similar to the ensemble-based subset-selection approach. This is interesting as both methods are fundamentally quite different in their underlying philosophy and technical implementation.

The optimization can equally be performed on one specific season if the shape of the distribution for the entire seasonal cycle is not of interest. Physically different regimes may be responsible for different parts of the cumulative distribution function. For instance, the hotter section of the distribution may be dominated by summer variability controlled by radiative physics, while the colder section may be dominated by winter events controlled by synoptic dynamics. Hence, by performing optimization on the full distribution, the analysis may be misinformed by model biases in irrelevant climatic regimes. A possible solution for this issue is to only use data from the relevant season for the optimization. This might additionally be of greater importance for rainfall extremes than temperature extremes, since the weather phenomena that bring about those extremes can be very different between summer and winter. However, the main conclusions of the paper remained unchanged when we optimized for June, July, and August temperatures (Figures S14–S16) or precipitation (Figures S17–S19) instead.

Biases in the shape were found to persist through time based on a series of model-as-truth experiments. A subset calibrated to have a distribution shape similar to a model-as-truth in-sample was found to lead to improved out-of-sample skill when calculating EPs or PsFB, even though those probabilities are only sensitive to the tail of the distributions. This is because EPs and PsFB are strongly influenced by shape bias. However, when calculating the PR, which is by definition the ratio of two EPs or PsFB, the bias correction methods were found to provide little to no identifiable improvement in skill (except for PRs characterizing the change in probability of warm extremes into the future). When taking the fraction of two EPs or PsFB, biased tail shapes play less of a role (one can consider the tail bias present in both the numerator and denominator to cancel) and the relative importance of trend bias begins to dominate, as confirmed by the toy model experiment. It is therefore theoretically possible for a PR to be fairly close to the truth even if their EPs or PsFB are not. This study explores an example where out-of-sample testing is highly beneficial and metric transitivity cannot simply be assumed. While evaluating the shapes of simulated distributions is clearly important, it is likely not the most important source of uncertainty around PR-based attribution statements and many metrics pertaining to extremes in a changing climate. Therefore, bias correction approaches that solely aim to correct for shape bias are likely to lead to only minor if not any reductions in biases in PR estimates, particularly for attribution statements pertaining to warm extremes. Note that the bias in temperature response to long-term changes in radiative forcing becomes increasingly important with increasing GHG forcing, while the shape bias is relatively static. The importance of a "correct" distribution shape only decreases as more rare extremes are analyzed, for example, for 1-in-5-year events (see Figure S9 and the toy model in Figure S13 in which PRs are even more sensitive to the trend than the shape when compared to 1-in-1-year events).

Since evaluating response bias to long-term changes in radiative forcing using multiple observational products is not common practice in the event attribution community, we suggest that the long-term response to forcing be evaluated and should be part of the optimization process if this characteristic of the raw model output is deemed unfit for purpose (in addition to distribution properties). The difficulty here however is that the nature of the long-term temperature response in-sample does not seem to persist out-of-sample (see, e.g., Figure 4 in Herger et al. (2018)). Knutti and Hegerl (2008) showed that it is possible for two climate models to very closely track historical warming trends but behave completely different thereafter (their Figure 4). This different behavior in the long-term warming is due to the counteracting effects of climate sensitivity, total forcing, and ocean heat uptake. Optimizing on trends within the instrumental period therefore will likely not constrain future projections. Note that calibrating on the PR itself will not necessarily help as the correct PR value could be obtained due to compensating errors (e.g., an appropriate combination of an overly narrow distribution and an underestimated trend). The toy model results could feed into the debate whether simulated trends should be preserved as they are (as, e.g., in Hempel et al., 2013) or bias corrected using observations (Maraun, 2016).

Future studies could test the sensitivity of results to different temporal resolutions and return periods of events. We additionally encourage the use of out-of-sample testing using long observational records and/or model-as-truth experiments to test bias correction approaches. It is critical that we identify whether there is in fact a gain in our ability to make out-of-sample predictions (i.e., Does the nature of the bias being corrected persist or does it break down in the projection period? Will the bias correction performed reduce bias in the metric we are interested in, only partly, or not at all?) As we have seen here, this is not guaranteed (also see Reichler & Kim, 2008; Reifen & Toumi, 2009). Fundamentally, bias correction is a statistical calibration exercise that will work in-sample by definition. Assessing whether or not it works out-of-sample is a critical step for evaluating the nature of extremes in a changing climate.

Acknowledgments
We would like to thank Jan Sedláček for providing access to the CMIP5 archive based at ETHZ. Nadja Herger, Oliver Angélil, and Markus Donat acknowledge the support of the Australian Research Council Centre of Excellence for Climate System Science (CE110001028) and Gab Abramowitz the Australian Research Council Centre of Excellence for Climate Extremes (CE170100023). We acknowledge the World Climate Research Programme's Working Group on Coupled Modelling, which is responsible for CMIP, and we thank the climate modeling groups (listed in Table S1 in the supporting information) for producing and making available their model output. For CMIP the U.S. Department of Energy's Program for Climate Model Diagnosis and Intercomparison provides coordinating support and led development of software infrastructure in partnership with the Global Organization for Earth System Science Portals. CMIP data can be obtained from http://cmip-pcmdi.llnl.gov/cmip5/. We use Python for data analysis and visualization.

References

Abramowitz, G., & Bishop, C. H. (2015). Climate model dependence and the ensemble dependence transformation of CMIP projections. *Journal of Climate*, *28*, 2332–2348. https://doi.org/10.1175/JCLI-D-14-00364.1

Alexander, L. V., Zhang, X., Peterson, T. C., Caesar, J., Gleason, B., Klein Tank, A. M. G., & Tagipour, A. (2006). Global observed changes in daily climate extremes of temperature and precipitation. *Journal of Geophysical Research*, *111*, D05109. https://doi.org/10.1029/2005JD006290

Anderson, T. W., & Darling, D. A. (1970). A test of goodness of fit. *Journal of the American Statistical Association*, *49*(268), 765–769.

Angélil, O., Perkins, S., Alexander, L., Stone, D., Donat, M., Wehner, M., et al. (2016). Comparing regional precipitation and temperature extremes in climate model and reanalysis products. *Weather and Climate Extremes*, *13*, 35–43. https://doi.org/10.1016/j.wace.2016.07.001

Angélil, O., Stone, D., Perkins, S., Alexander, L. V., Wehner, M., Shiogama, H., et al. (2018). On the nonlinearity of spatial scales in extreme weather attribution statements. *Climate Dynamics*, *50*(7–8), 2739–2752. https://doi.org/10.1007/s00382-017-3768-9

Angélil, O., Stone, D., Wehner, M. F., Paciorek, C. J., Krishnan, H., & Collins, W. D. (2017). An independent assessment of anthropogenic attribution statements for recent extreme temperature and rainfall events. *Journal of Climate*, *30*(1), 5–16. https://doi.org/10.1175/JCLI-D-16-0077.1

Bellprat, O., & Doblas-Reyes, F. (2016). Attribution of extreme weather and climate events overestimated by unreliable climate simulations. *Geophysical Research Letters*, *43*, 2158–2164. https://doi.org/10.1002/2015GL067189

Borodina, A., Fischer, E. M., & Knutti, R. (2017). Potential to constrain projections of hot temperature extremes. *Journal of Climate*, *30*, 9949–9964. https://doi.org/10.1175/JCLI-D-16-0848.1

Christensen, J. H., Boberg, F., Christensen, O. B., & Lucas-Picher, P. (2008). On the need for bias correction of regional climate change projections of temperature and precipitation. *Geophysical Research Letters*, *35*, L20709. https://doi.org/10.1029/2008GL035694

Collins, M., & Knutti, R. (2013). Chapter 12—Long-term climate change: Projections, commitments and irreversibility. In T. F. Stocker, et al. (Eds.), *Climate change 2013: The physical science basis. Contribution of Working Group I to the Fifth Assessment Report of the Intergovernmental Panel on Climate Change* (pp. 1029–1136). Cambridge, UK: Cambridge University Press. https://doi.org/10.1017/CBO9781107415324.024

Donat, M. G., Pitman, A. J., & Seneviratne, S. I. (2017). Regional warming of hot extremes accelerated by surface energy fluxes. *Geophysical Research Letters*, *44*, 7011–7019. https://doi.org/10.1002/2017GL073733

Ehret, U., Zehe, E., Wulfmeyer, V., Warrach-Sagi, K., & Liebert, J. (2012). HESS opinions "Should we apply bias correction to global and regional climate model data?". *Hydrology and Earth System Sciences*, *16*(9), 3391. https://doi.org/10.5194/hess-16-3391-2012

Gurobi Optimization, Inc. (2015). Gurobi optimizer reference manual. Retrieved from http://www.gurobi.com

Harris, I., Jones, P. D., Osborn, T. J., & Lister, D. H. (2014). Updated high-resolution grids of monthly climatic observations—The CRU TS3.10 dataset. *International Journal of Climatology*, *34*, 623–642. https://doi.org/10.1002/joc.3711

Hartmann, D. J., Klein Tank, A. M. G., Rusticucci, M., Alexander, L., Brönnimann, S., Charabi, Y. A.-R., et al. (2013). Observations: Atmosphere and surface, climate change 2013: The physical science basis, *Contribution of Working Group I to the Fifth Assessment Report of the Intergovernmental Panel on Climate Change* (pp. 159–254). Cambridge, UK: Cambridge University Press. https://doi.org/10.1017/CBO9781107415324.008

Hauser, M., Gudmundsson, L., Orth, R., Jézéquel, A., Haustein, K., Vautard, R., et al. (2017). Methods and model dependency of extreme event attribution: The 2015 European drought. *Earth's Future*, *5*, 1–10. https://doi.org/10.1002/2017EF000612

Hempel, S., Frieler, K., Warszawski, L., Schewe, J., & Piontek, F. (2013). A trend-preserving bias correction the ISI-MIP approach. *Earth System Dynamics*, *4*(2), 219–236. https://doi.org/10.5194/esd-4-219-2013

Heo, J. H., Shin, H., Nam, W., Om, J., & Jeong, C. (2013). Approximation of modified Anderson-Darling test statistics for extreme value distributions with unknown shape parameter. *Journal of Hydrology*, *499*, 41–49. https://doi.org/10.1016/j.jhydrol.2013.06.008

Herger, N., Abramowitz, G., Knutti, R., Angélil, O., Lehmann, K., & Sanderson, B. M. (2018). Selecting a climate model subset to optimise key ensemble properties. *Earth System Dynamics*, *9*, 135–151. https://doi.org/10.5194/esd-9-135-2018

Herring, S. C., Hoell, A., Hoerling, M. P., Kossin, J. P., Schreck, C. J. III, & Stott, P. A. (2016). Explaining extreme events of 2015 from a climate perspective. *Bulletin of the American Meteorological Society*, *97*(12), S102–S102.

Herring, S. C., Hoerling, M. P., Kossin, J. P., Peterson, T. C., & Stott, P. A. (2015). Explaining extreme events of 2014 from a climate perspective. *Bulletin of the American Meteorological Society*, *96*(12), S1–S172.

Herring, S. C., Hoerling, M. P., Peterson, T. C., & Stott, P. A. (2014). Explaining extreme events of 2013 from a climate perspective. *Bulletin of the American Meteorological Society*, *95*(9), S1–S96.

Jeon, S., Paciorek, C. J., & Wehner, M. F. (2016). Quantile-based bias correction and uncertainty quantification of extreme event attribution statements. *Weather and Climate Extremes*, *12*, 24–32. https://doi.org/10.1016/j.wace.2016. 02.001

King, A. D., & Karoly, D. (2017). Climate extremes in Europe at 1.5 and 2 degrees of global warming. *Environmental Research Letters*, *12*, 114031. https://doi.org/10.1088/1748-9326/aa8e2c

King, A. D., Karoly, D. J., & Henley, B. J. (2017). Australian climate extremes at 1.5°C and 2°C of global warming. *Nature Climate Change*, *7*(6), 412–416. https://doi.org/10.1038/nclimate3296

Knutti, R., & Hegerl, G. C. (2008). The equilibrium sensitivity of the Earth's temperature to radiation changes. *Nature Geoscience*, *1*(11), 735–743. https://doi.org/10.1038/ngeo337

Knutti, R., Sedláček, J., Sanderson, B. M., Lorenz, R., Fischer, E., & Eyring, V. (2017). A climate model projection weighting scheme accounting for performance and interdependence. *Geophysical Research Letters*, *44*, 1909–1918. https://doi.org/10.1002/2016GL072012

Lewis, S. C., & King, A. D. (2015). Dramatically increased rate of observed hot record breaking in recent Australian temperatures. *Geophysical Research Letters*, *42*, 7776–7784. https://doi.org/10.1002/2015GL065793

Lewis, S. C., & King, A. D. (2017). Evolution of mean, variance and extremes in 21st century temperatures. *Weather and Climate Extremes*, *15*, 1–10. https://doi.org/10.1016/j.wace.2016.11.002

Li, H., Sheffield, J., & Wood, E. F. (2010). Bias correction of monthly precipitation and temperature fields from Intergovernmental Panel on Climate Change AR4 models using equidistant quantile matching. *Journal of Geophysical Research*, *115*, D10101. https://doi.org/10.1029/2009JD012882

Macias-Fauria, M., Seddon, A. W., Benz, D., Long, P. R., & Willis, K. (2014). Spatiotemporal patterns of warming. *Nature Climate Change*, *4*(10), 845–846. https://doi.org/10.1038/nclimate2372

Maraun, D. (2016). Bias correcting climate change simulations—A critical review. *Current Climate Change Reports*, *2*(4), 211–220. https://doi.org/10.1007/s40641-016-0050-x

Patz, J. A., Campbell-Lendrum, D., Holloway, T., & Foley, J. A. (2005). Impact of regional climate change on human health. *Nature*, *438*(7066), 310. https://doi.org/10.1038/nature04188

Perkins-Kirkpatrick, S. E., & Gibson, P. B. (2017). Changes in regional heatwave characteristics as a function of increasing global temperature. *Scientific Reports*, *7*(1), 12256. https://doi.org/10.1038/s41598-017-12520-2

Peterson, T. C., Hoerling, M. P., Stott, P. A., & Herring, S. C. (2013). Explaining extreme events of 2012 from a climate perspective. *Bulletin of the American Meteorological Society*, *94*(9), 1–74.

Peterson, T. C., Stott, P. A., & Herring, S. C. (2012). Explaining extreme events of 2011 from a climate perspective. *Bulletin of the American Meteorological Society*, *93*(7), 1041–1067. https://doi.org/10.1175/BAMS-D-12-00021.1

Piani, C., Haerter, J. O., & Coppola, E. (2010). Statistical bias correction for daily precipitation in regional climate models over Europe. *Theoretical and Applied Climatology*, *99*(1–2), 187–192. https://doi.org/10.1007/s00704-009-0134-9

Piani, C., Weedon, G. P., Best, M., Gomes, S. M., Viterbo, P., Hagemann, S., & Haerter, J. O. (2010). Statistical bias correction of global simulated daily precipitation and temperature for the application of hydrological models. *Journal of Hydrology*, *395*(3), 199–215. https://doi.org/10.1016/j.jhydrol.2010.10.024

Reichler, T., & Kim, J. (2008). How well do coupled models simulate today's climate?*Bulletin of the American Meteorological Society*, *89*(3), 303–311. https://doi.org/10.1175/BAMS-89-3-303

Reifen, C., & Toumi, R. (2009). Climate projections: Past performance no guarantee of future skill?*Geophysical Research Letters*, *36*, L13704. https://doi.org/10.1029/2009GL038082

Sanderson, B. M., Wehner, M., & Knutti, R. (2017). Skill and independence weighting for multi-model assessments. *Geoscientific Model Development*, *10*, 2379–2395. https://doi.org/10.5194/gmd-10-2379-2017

Sanderson, B. M., Xu, Y., Tebaldi, C., Wehner, M., O'Neill, B., Jahn, A., et al. (2017). Community climate simulations to assess avoided impacts in 1.5 and 2°C futures. *Earth System Dynamics*, *8*(3), 827. https://doi.org/10.5194/esd-8-827-2017

Seneviratne, S., Nicholls, N., Easterling, D. R., Goodess, C., Kanae, S., Kossin, J., et al. (2012). Changes in climate extremes and their impacts on the natural physical environment. Managing the risk of extreme events and disasters to advance climate change adaptation, *A special report of Working Groups I and II of the IPCC, Annex II* pp. 109–230). Cambridge, UK: Cambridge University Press.

Sillmann, J., Kharin, V. V., Zwiers, F. W., Zhang, X., & Bronaugh, D. (2013). Climate extremes indices in the CMIP5 multimodel ensemble: Part 2. Future climate projections. *Journal of Geophysical Research: Atmospheres*, *118*, 2473–2493. https://doi.org/10.1002/jgrd.50188

Sippel, S., Otto, F. E. L., Forkel, M., Allen, M. R., Guillod, B. P., Heimann, M., et al. (2016). A novel bias correction methodology for climate impact simulations. *Earth System Dynamics*, *7*, 71–88. https://doi.org/10.5194/esd-7-71-2016

Stephens, M. A. (1970). Use of the Kolmogorov-Smirnov, Cramer-Von Mises and related statistics without extensive tables. *Journal of the Royal Statistical Society*, *32*, 115–122.

Taylor, K. E., Stouffer, R. J., & Meehl, G. A. (2012). An overview of CMIP5 and the experiment design. *Bulletin of the American Meteorological Society*, *93*(4), 485–498. https://doi.org/10.1175/BAMS-D-11-00094.1

Wang, C., Zhang, L., Lee, S. K., Wu, L., & Mechoso, C. R. (2014). A global perspective on CMIP5 climate model biases. *Nature Climate Change*, *4*(3), 201. https://doi.org/10.1038/nclimate2118